Experimental study of the asymmetric charge transfer reaction between Ar^+ ions and Fe atoms

I. Korolov,[1,a)] G. Bánó,[1,2] Z. Donkó,[1] A. Derzsi,[1] and P. Hartmann[1]
[1]*Research Institute for Solid State Physics and Optics of the Hungarian Academy of Sciences, H-1525 Budapest, POB 49, Hungary*
[2]*Department of Biophysics, P J Šafarik University in Košice, 04001 Jesenna 5, Košice, Slovakia*

(Received 3 November 2010; accepted 28 December 2010; published online 9 February 2011)

We investigate the Ar^+–Fe asymmetric charge transfer (ACT) reaction using a combination of plasma diagnostics methods and a kinetic model of the afterglow plasma, which allow monitoring of the temporal evolution of the densities of different species. The iron vapor is created inside a discharge cell by cathode sputtering; its density is measured by atomic absorption spectroscopy. The rate coefficient of the reaction is evaluated from the emission intensity decay of Fe^{+*} lines pumped by the ACT process in the He–Ar–Fe and Ar–Fe afterglow plasmas. The measurements yield a rate coefficient $k = 7.6(\pm 3.0) \times 10^{-9}$ cm^3 s^{-1} at $T = 300$ K. © *2011 American Institute of Physics*. [doi:10.1063/1.3548657]

I. INTRODUCTION

Charge transfer reactions are well known to influence the chemistry and the ion kinetics in gaseous discharges. Such reactions can be symmetric (when gas ions react with the atoms or molecules of the parent gas) or asymmetric (when the reacting particles are of different types). In particular, reactions between ground state noble gas ions (A^+) and metal atoms (M) play an important role in many glow discharge applications, such as various hollow cathode lamps,[1,2] analytical plasma sources,[3–10] as well as different metal ion lasers (e.g., Ne–Cu^+, He–Ag^+, He–Au^+, He–Cu^+, and He–Zn^+) (Refs. 11–16). Despite their importance, our knowledge about the reaction rates of these processes is rather limited (due to difficulties associated with the creation of metal vapor of controlled density), compared to the reaction rates between gaseous species, which have thoroughly been investigated.[17–20]

Symmetric charge transfer processes are resonant reactions. Asymmetric processes are nonresonant, in most cases the levels of the collision partner lying $\Delta E \cong 0.1$–0.3 eV below the energy of the colliding ion are excited with the highest probability.[21] It has to be noted that in special cases, such as in the $He_2^+ + Ar$ charge transfer process (which is followed by dissociation) such a close energy match is not required.

During the asymmetric charge transfer (ACT) reactions of interest here, a ground state metal atom is ionized and excited in a single step,

$$A^+ + M \longrightarrow A + M^{+*} + \Delta E. \quad (1)$$

Most of the earlier rate coefficient measurements of ACT reactions between noble gas ions and metal atoms were carried out with volatile metals, such as Hg, Pb, Cd, Zn, or Tl.[22–26] There are very few rate coefficient and cross-section data available for other elements, that are difficult to evaporate, e.g., Cu, Fe, Ti, Ni, and Mo. For the Ne–Cu^+ system, data have been published[27] for thermal energies (~2000 K). Cross sections for the interaction of Xe^+ ions and various metals have been determined for a wide range of ion energies 1 eV $\leq \varepsilon \leq$ 5000 eV.[28] To our best knowledge, there are no experimental cross section or rate coefficient data available for ACT reactions between Ar^+ ions and metal atoms at thermal energies, which are of high importance in many glow discharge applications.[8,9]

In this paper we report our experimental investigation of the ACT process between argon ions and iron atoms and the determination of its rate coefficient. There are several levels of Fe^{+*} that can be populated by ACT with Ar^+ ions; therefore, the reaction is expected to be fast. Evidence for the ACT reaction between these species has been given by other authors, see Refs. 29–33; however, the rate coefficient of the reaction has not been measured yet to our best knowledge. As to theoretical efforts, the semiclassical calculations of ACT rate coefficients between Ar^+ ions and different metal atoms by Bogaerts *et al.*[34] have to be mentioned. Their typical calculated rate coefficients are in the range of $k = 10^{-10}$–10^{-8} cm^3 s^{-1}; for iron, a value of 13.76×10^{-9} cm^3 s^{-1} has been given.

Here, our aim is to determine this rate coefficient experimentally. In Sec. II we describe the experimental apparatus and the plasma diagnostics methods (Langmuir probe measurements, emission and absorption spectroscopy) as well as the principle of the determination of the ACT rate coefficient measurement. In Sec. III we present and discuss the experimental data, while Sec. IV gives a concise summary of the work.

II. EXPERIMENTAL

The rate coefficient of the ACT reaction between argon ions and iron atoms is measured in a stationary afterglow experiment. The metal (Fe) vapor is generated by means of cathode sputtering in a pulsed glow discharge operated either in the He–Ar mixture or in pure Ar buffer gas. The

a)Electronic mail: Ihor.Korolov@gmail.com.

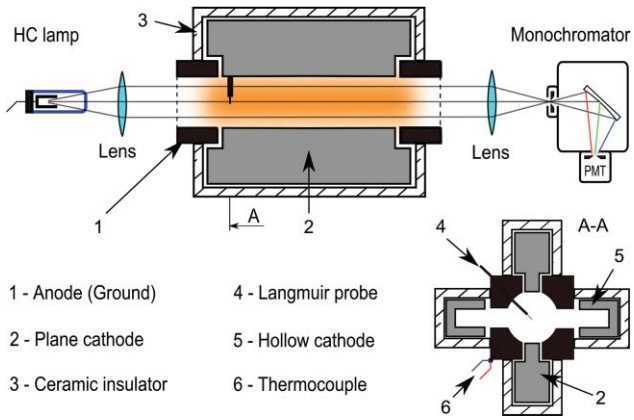

FIG. 1. Schematic view of the reaction cell and the optical setup. The A–A section is perpendicular to the optical axis.

measurement of the decay rate of the Ar^+ ion density (monitored by the intensity of Fe-II lines excited by ACT) during the afterglow period at different metal atom concentrations allows the evaluation of the ACT rate coefficient.

A. Discharge cell and vacuum system

The discharge cell (see Fig. 1)—situated inside a vacuum chamber—consists of two plane cathodes (PCs) and two hollow cathodes (HCs), which are used to create the plasma and the metal vapor with densities in a wide range. Only the set of PCs is used in the experiments presented in this paper. The cathodes are made of pure (>99.8%) iron; their active area is 50 mm (length) × 5 mm (width). The inner diameter and the length of the anode cavity are 15 and 70 mm, respectively. The discharges are operated in a pulsed regime, with a typical pulse duration of 1–2 ms. During the measurements the temperature of the cell is monitored using a K-type thermocouple installed inside the anode body.

The vacuum system is sketched in Fig. 2. The working pressure (1–20 mbar) is monitored by a capacitance pressure gauge. Because of the high purity requirements, prior to the measurements, the discharge chamber and the gas tubing are heated, while pumping, above 480 K to evaporate volatile impurities from the walls. Before the experiments the main chamber is evacuated below 5×10^{-9} mbar by a turbomolecular pump. The experiments are performed using 6.0 purity argon and helium gases (further purified using liquid nitrogen traps and a VICI® P100-2 purifier) with a slow gas flow, up to 30 sccm, measured and controlled by flow meters/controllers. The effect of impurities and the estimation of the cleanliness level of the system are discussed in Sec. II D 3.

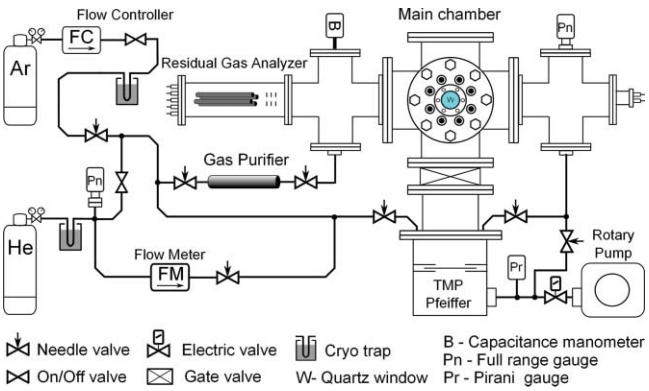

FIG. 2. The vacuum system of the apparatus.

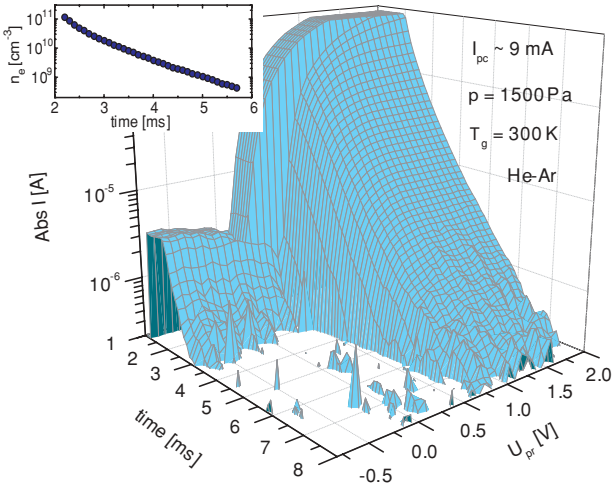

FIG. 3. An example of the time evolution of the probe characteristic during a discharge pulse (of length 1.8 ms) and the subsequent afterglow period in the He–2%Ar mixture. Inset: time dependence of electron density.

B. Langmuir probe measurements

In our experiments Langmuir probe measurements[35–39] are carried out to gain a better understanding of the plasma processes during the afterglow period: (i) to validate the results of the kinetic model (Sec. II D 1), (ii) to test the gas purity in the discharge cell (Sec. II D 3), and (iii) to get information on the electron temperature of the decaying plasma.

The Langmuir probe (made of a 20 μm W wire with a length of 2.5 mm) is situated at a fixed position inside the discharge cell (see Fig. 1). The probe support consists of two coaxial glass tubes with the diameter of the outer one being ~0.6 mm. To avoid the formation of an electrical contact between the probe and the metal layer deposited onto the outer support surface, the inner glass tube is made 1 mm shorter as compared to the outer one (see also Ref. 35). During the measurements the probe surface is periodically cleaned by ion bombardment applying a negative bias voltage of ~80 V during the discharge pulses (with a typical cleaning current of 1–3 mA). An example of a measured time-resolved probe characteristic is shown in Fig. 3 for a discharge (with 9 mA current and 1.8 ms pulse length) and subsequent afterglow period in the He–2%Ar mixture.

The electron density at a given time is obtained from the electron current part of the probe characteristic in the acceleration region using the "I-squared" method.[36] An example of the calculated electron density decay is shown in the inset of Fig. 3. The electron temperature T_e and the electron energy distribution function are determined from the second derivative of the characteristic.

C. Fe density measurements

The density of sputtered iron atoms inside the cell is determined using atomic absorption spectroscopy. An iron–neon hollow cathode lamp (type: L233-26NU) is used as a light source. For detection we use an Acton VM-502 monochromator (20 cm focal length, 1200 grooves/mm grating providing a resolution of 0.08 nm at a slit width of 20 μm) equipped with a Hamamatsu (H7732P-11) photomultiplier tube of which the signal is recorded in a time-resolved photon counting mode by an AMETEK multi channel scaler pci-card (see Fig. 1). During the experiments the emission intensity of the Fe-I 372.0 nm line passing through the discharge cell is measured with (I) and without (I_0) iron vapor present inside the cell. The absorbance is calculated as $A = \ln(I_0/I)$. We have found that for lamp currents below 8 mA the absorbance does not depend on the lamp current. To avoid self-absorption[40] and to optimize the emission line profile, the current of the lamp is set to 5 mA. The expected temperature of the metal vapor inside the HC lamp is 350 ± 50 K.[41] The highest absorbance observed during the measurements was 0.25, which is within the validity of the Lambert–Beer law.[40] To obtain accurate temporal profiles of the absorption and emission signals, averaging was carried out for 1000–7000 pulses, depending on the intensity of the signals.

The iron density N is calculated using the following equation:[42]

$$N = \frac{2\varepsilon_0\sqrt{\pi}m_e c}{e^2 \ln(e)\sqrt{\ln 2}} \frac{A\Delta\nu_D}{\Phi l f}, \tag{2}$$

where $\Delta\nu_D$ is the Doppler width of the absorption line (taken to be 1.44×10^9 Hz), $l = 0.05$ m is the effective path length, ε_0 is the permittivity of vacuum, and m_e and c are the electron mass and the speed of light, respectively. The oscillator strength $f = 0.0411$ is taken from Refs. 43 and 44. The line-profile factor Φ expresses the departure of the measured absorbance from the idealized case of an unsplit pure Doppler broadened absorption line and a monochromatic emission line.[42] This factor is calculated from the measured hyperfine structure of the Fe-I 372.0 nm resonance line[45] and is found to be $\approx$1.

The accuracy of the derived ACT rate coefficient is mainly determined by the uncertainty of the absorption measurement. This latter originates from several sources: (i) pressure and Stark broadening effects not taken into account (estimated to introduce an error of <5%), (ii) low-lying metastable states of Fe contributing to the asymmetric charge transfer but not detected in the atomic absorption measurement [at our relatively high pressure conditions this is expected to introduce an error of not more than 5% (Ref. 46)] as well as (iii) uncertainties in some of the physical parameters (e.g., oscillator strength and Doppler width) used in Eq. (2). We expect the total error of the metal density measurements to be approximately 25%–30%.

Typical time-dependent decays of the measured iron density during the afterglow period of the pulsed discharges (in He–2%Ar mixture, at a pressure of 1500 Pa) are plotted in Fig. 4 for three different discharge currents.

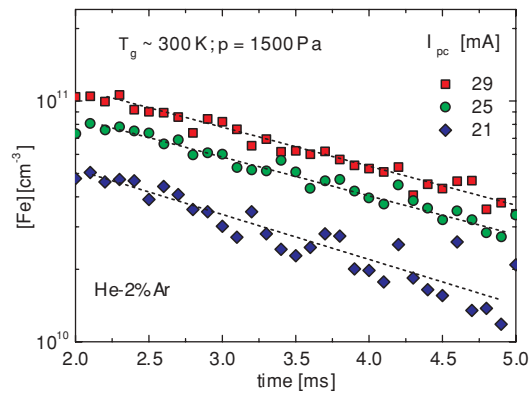

FIG. 4. Ground state iron concentration derived from the measured absorbance of the Fe-I 372.0 nm line during the afterglow period of the pulsed discharges (1.8 ms pulse length and 3 Hz repetition rate) at a series of discharge currents (I_{pc}) and different conditions indicated.

D. Plasma formation and rate coefficient measurements

In the present experiments Ar^+ ions are produced inside the discharge cell by running discharges under two different plasma conditions: (i) in a He–2%Ar buffer gas mixture and (ii) in pure Ar gas. In the following we describe these two different types of discharges, introduce a kinetic model to follow the time-evolution of the densities of plasma species, discuss the way of the determination of the ACT reaction rate coefficient, and address the effect of impurities.

1. Discharges in He–Ar mixtures

During the active discharge in He–Ar buffer gas mixtures, mainly He^+ ions and He^m metastable atoms are formed. During the afterglow, due to the relatively high buffer gas pressure (1400–1800 Pa), the He^+ ions are first converted to He_2^+ ions (via three body association processes). Next, an Ar^+ dominated plasma is formed in a sequence of ion molecule reactions, including ACT reactions of He_2^+ ions with Ar atoms and Penning ionization collisions of Ar atoms with He^m metastable atoms. Such an afterglow plasma becomes thermal,[36,39] $T_{ion} \approx T_e \approx T_{gas} \approx 300$ K (proved also by Langmuir probe and the thermocouple measurements) approximately 0.5 ms after switching the discharge off. The fast thermalization is mostly related to the fact that He^m metastables are converted to Ar ions, which hinder them to produce fast electrons in metastable–metastable collisions. This is the main advantage of using the He–Ar mixture.

To gain a better understanding of the details of plasma processes inside the cell and to optimize the experiments, a numerical kinetic model of the afterglow period has been developed. An example of calculated plasma evolution of the discharge afterglow is shown in Fig. 5. The ion and metastable reactions taken into account in this model are given in Table I. The diffusion coefficients of the ions were calculated using measured reduced zero-field mobilities in helium and argon.[47]

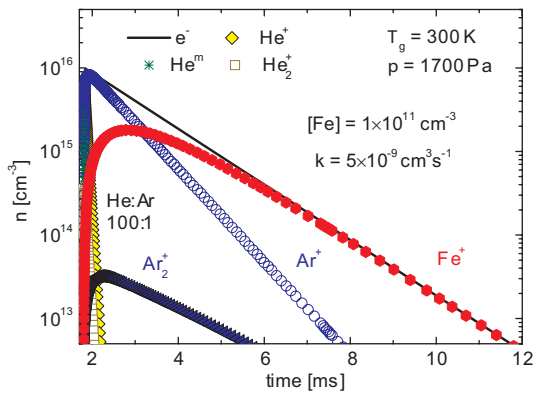

FIG. 5. Time evolution of the densities of different plasma species during the afterglow in the discharge cell calculated with the kinetic model in the He–1%Ar mixture. The iron atom density is taken to be constant and the ACT reaction rate is assumed to be $k = 10^{-9}$ cm^3 s^{-1}. Note the rapid decay of the density of all helium species.

Once the formation of Ar^+ ions is completed (at about 0.5 ms in Fig. 5), the balance equation for their density, $[Ar^+]$, can be written in the following form:

$$\frac{d[Ar^+]}{dt} = -k[Ar^+][Fe] - \frac{D}{\Lambda^2}[Ar^+], \tag{3}$$

where the first term on the right hand side represents the ACT reaction between Ar^+ ions and Fe atoms with a rate coefficient k, the second term is the ambipolar diffusion to the wall with a diffusion constant D and a characteristic diffusion length Λ. Assuming a constant iron number density [Fe]—which is a reasonable approximation for short ($\leq$ 1 ms) time segments—the solution of Eq. (3) can be written as

$$[Ar^+]_t = [Ar^+]_0 \exp(-t/\tau), \tag{4}$$

where

$$1/\tau = \frac{D}{\Lambda^2} + k[Fe]. \tag{5}$$

TABLE I. The main reactions and corresponding rate coefficients considered in the model. The rate coefficients for two-body processes are given in units of cm^3 s^{-1} and for three-body processes in cm^6 s^{-1}. A temperature T = 300 K is assumed.

Reaction	Rate	Reference
$He^+ + He + He \rightarrow He_2^+ + He$	1×10^{-31}	48
$He^m + He^m \rightarrow He^+ + He + e^-$	5×10^{-9}	49
$He^m + He^m \rightarrow He_2^+ + e^-$	5×10^{-9}	50
$He_2^+ + e^- \rightarrow 2He$	$<3 \times 10^{-10}$	51
$He^+ + Ar \rightarrow Ar^+ + He$	1×10^{-13}	48
$He^m + Ar \rightarrow Ar^+ + He + e^-$	7×10^{-11}	52
$He_2^+ + Ar \rightarrow Ar^+ + 2He$	2×10^{-10}	48
$Ar^+ + Ar + He \rightarrow Ar_2^+ + He$	1.3×10^{-31}	53
$Ar_2^+ + e^- \rightarrow 2Ar$	8×10^{-7}	54
$Ar^m + Ar^m \rightarrow Ar^+ + Ar + e^-$	6.3×10^{-10}	55
$Ar^m + Ar^m \rightarrow Ar_2^+ + e^-$	5.7×10^{-10}	55
$Ar^+ + Ar + Ar \rightarrow Ar_2^+ + Ar$	2.7×10^{-31}	56
$Ar^m + Fe \rightarrow Fe^+ + Ar + e^-$	2.3×10^{-10}	34
$Ar^+ + Fe \rightarrow Fe^+ + Ar$	$(1–20) \times 10^{-9}$[a]	...

[a]This is the ACT reaction rate to be determined in our experiments. In the model we have scanned the above range of the rate to find proper experimental conditions.

Here $[]_t$ denotes time dependence. The first term on the right side of Eq. (5) is a constant. Thus, the plot of $1/\tau$ versus the iron number density, [Fe], will be a straight line, the slope of which is given by the rate coefficient k. The absolute value of the iron number density, needed for the evaluation of k, is provided by the atomic absorption measurements. On the other hand, we do not need the absolute density of argon ions, the characteristic decay time τ can be obtained from relative values. In our experiment, the relative number density of argon ions is determined from the intensity (I_{CT}) of Fe-II lines pumped by the ACT reaction between the Ar^+ ions and the Fe atoms. The intensity of these lines is directly proportional to $[Ar^+]_t[Fe]_t$. It follows that the relative Ar^+ ion density decay can be obtained from the ratio of $I_{CT}/[Fe]_t$, or I_{CT}/A, where A is the measured absorbance of Fe atoms. Fitting the time evolution of this ratio by an exponential decay gives us the value of τ.

2. Discharges in pure Ar

In the case of pure argon discharges one has to be aware that argon metastable atoms, which are not destroyed rapidly during the afterglow, can serve as an additional source of Ar ions and fast electrons via $Ar^m + Ar^m$ collisions. As a consequence, Eq. (4) becomes invalid, and the plasma is not thermalized rapidly after switching the discharge off. Moreover, at high pressures argon ions can be converted to Ar_2^+ ions.

Our kinetic model indicates that for relatively low pressures (200–300 Pa), the influence of Ar_2^+ ions, Ar^m metastables, and the slowly cooling electron temperature $T_e(t)$ on the Ar^+ decay is negligible during the very first few milliseconds period of the afterglow. Thus, in contrast to the He–Ar plasma (where it takes about 0.5 ms to form the Ar^+ dominated afterglow), the evaluation of k in pure argon discharges has to be carried out in the very early afterglow. Apart from this peculiarity, the data evaluation proceeds in the same way as described for He–Ar discharges.

3. Effect of impurities

In our afterglow plasma the decay of the ion and electron density is caused mainly by ambipolar diffusion and by reactions with impurities followed by fast recombination.[57] This way impurities influence the density of argon ions via an additional loss channel. Under quasineutral conditions the level of impurities can be estimated by measuring the decay time of the electron density by the Langmuir probe. In He–2%Ar mixture at $p = 1500$ Pa and $T = 300$ K, in the Ar^+ dominated afterglow plasma of a low current (~4 mA) pulsed discharge, we typically obtained a purity level below 0.8 ppm (parts per million). As long as the level of impurities is kept so low and constant during the experiments, the reactions of argon ions with impurities add only a small constant to the right hand side of Eq. (5), which does not affect the value of k determined by the evaluation procedure described above. To ensure that the measurements are carried out under proper conditions, purity tests relying on the Langmuir probe electron density measurements in Ar^+-dominated afterglow

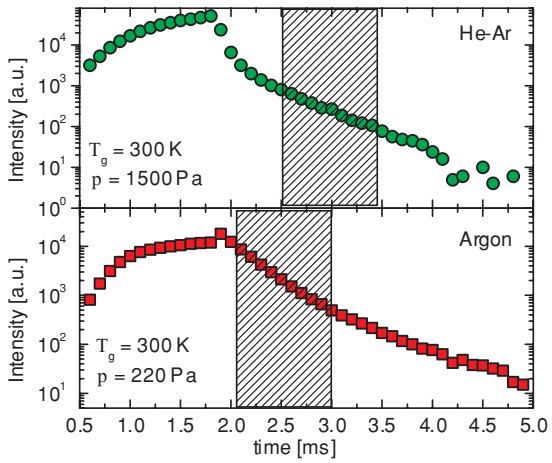

FIG. 6. Measured emission intensity of the 249.1 nm Fe-II charge transfer-excited line in the He–2%Ar (upper panel) and Ar (lower panel) afterglow plasmas averaged over 5000 pulses. The PC discharge pulses are 1.8 ms long with a repetition rate of 3 Hz. $I_{pc} = 25$ mA. The hatched rectangles represent the time intervals during which the characteristic decay time of Ar^+ ions is determined. The falling edge of the current pulses is shorter than 30 μs.

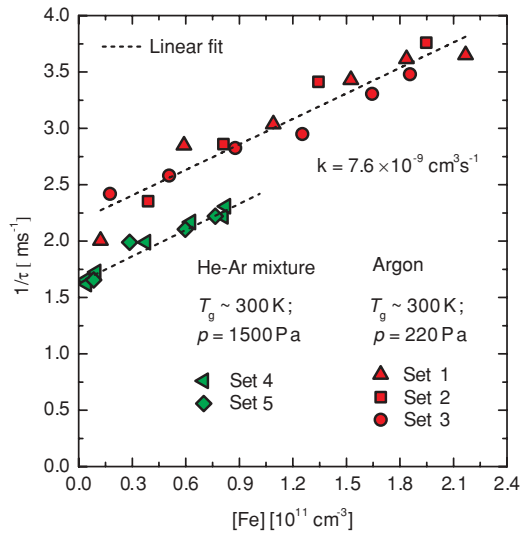

FIG. 7. Dependence of the characteristic decay time of $[Ar^+]$ on [Fe] during the afterglow period.

plasmas are always performed at the beginning and at the end of the measurements.

III. EXPERIMENTAL RESULTS AND DISCUSSION

Iron ions have several excited states with energies right below the energy of ground state Ar^+ ions (within 1 eV), which are thus suitable for ACT reaction. There are numerous Fe-II transitions[29,30] (e.g., 249.1, 275.7, 247.8, and 275.3 nm) originating from these levels, which are efficiently excited by the ACT reaction. Assuming that the ACT reaction strongly dominates over other (e.g., electron impact) excitation channels of these transitions and that the emission lifetimes are much shorter than the characteristic decay of the afterglow plasma, the intensities of all these ACT-excited lines are proportional to the Fe atom and Ar^+ ion number densities during the afterglow. It follows that all the ACT-excited lines have the same relative decay in the afterglow, as it was indeed confirmed by our measurements at identical discharge conditions (pressure, current, etc.).

Examples of the measured 249.1 nm line intensities in the He–2%Ar and Ar afterglow plasmas are shown in Fig. 6. The fast decay of the ACT-excited line in the He–2%Ar mixture within ≤0.5 ms after switching the discharge off is (i) due to plasma relaxation (electron and ion temperature), not included in our kinetic model and (ii) due to the possible pumping of Fe^{+*} levels by He^+, He^m, and He_2^+ ions, which quickly disappear (see Fig. 5). In the case of the pure Ar plasma, the fast decay is not observed. The hatched rectangles in Fig. 6 represent the time intervals during which the characteristic decay time of Ar^+ ions is determined.

Both, the intensity measurements of ACT-excited lines, $I_{CT}(t)$, and the detection of the Fe atomic absorbance $A(t)$ are synchronized with the discharge pulses. Thus, the time evolution of the relative Ar^+ ion density during the afterglow is readily obtained from the ratio of $I_{CT}(t)/A(t)$. In principle, the Ar^+ ion density decay obeys the exponential form of Eq. (4) only when there is a constant metal density present in the cell. Although the iron density gradually decreases during the afterglow, within a relatively short time interval (typically 0.5–1 ms, see Fig. 6) used for fitting the Ar^+ ion density decay, it does not vary more than ±10%–15%. Thus, during this short period of time [Fe] is approximated by a constant (average) value and the Ar^+ ion density decay is fitted by a single exponential function. During the course of measurements the discharge current, I_{pc}, is set to different values (ranging from 5 to 30 mA), which results in different metal atom densities. The frequency and the width of the discharge pulses are set in a way that the temperature of the discharge cell is kept nearly constant (300 ± 3 K) for the different discharge current values.

The measured dependence of the characteristic decay time of Ar^+ ions on the iron atom density is shown in Fig. 7 for discharges in the He–2%Ar mixture (1500 Pa) and in pure Ar buffer gas (220 Pa). The different data sets in this figure represent results taken on different days—confirming a good reproducibility of the measurements. It is evident that the data points of $1/\tau$ versus metal density give a straight line, for both He–2%Ar and Ar buffer gases, with the same slope of

$$k = 7.6(\pm 3.0) \times 10^{-9} \mathrm{cm}^3\,\mathrm{s}^{-1},$$

which is the rate coefficient of the ACT reaction [see Eq. (5)]. The vertical shift of the two fitted lines originates from the different speed of diffusion of Ar^+ ions in He–Ar and Ar buffer gases. The fact that these lines are parallel (within the limits of accuracy) adds confidence to the measured reaction rate value. As already mentioned earlier, the estimated error of 35%–40% in the ACT rate is mainly due to the uncertainties in the iron number density determination inside the cell.

Based on the above results, we conclude that the ACT reaction between Ar^+ ions and Fe atoms plays an important role in the ionization of iron atoms in Ar–Fe discharges. For instance, the rate coefficient calculated by Bogaerts *et al.*[34] for Penning ionization of Fe atoms by Ar^m metastables is 2.3×10^{-10} cm^3 s^{-1}, which is more than 1 order of

magnitude lower than the measured rate for the ACT reaction. Bogaerts *et al.*[34] have also calculated ACT rate coefficients: for the Ar–Fe system they gave a value of the rate coefficient (13.76×10^{-9} cm^3 s^{-1}), which is about a factor of 2 higher than our measured value. However, when calculating the relative sensitivity factors in glow discharge spectroscopy they have used a four times lower rate coefficient value (3.44×10^{-9} cm^3 s^{-1}) to get a reasonable agreement with the experiments.

IV. SUMMARY

We have developed an experimental apparatus to investigate the asymmetric charge transfer reaction between Ar^+ ions and Fe atoms. The combination of different plasma diagnostics methods (emission and absorption spectroscopy as well as Langmuir probe measurements) with a kinetic model of the plasma processes made it possible to determine the rate coefficient of the asymmetric charge transfer process between Ar^+ ions and Fe atoms. The measurements were carried out in the afterglow of pulsed, plane cathode sputtering discharges in Ar and He–Ar mixtures at pressures of 220 and 1500 Pa, respectively. The value of the ACT rate coefficient was determined to be $7.6(\pm 3.0) \times 10^{-9}$ cm^3 s^{-1} at $T = 300$ K. The experimental apparatus and the analysis techniques developed and presented here are planned to be used for further studies of the ACT reactions between other elements.

ACKNOWLEDGMENTS

The authors gratefully acknowledge the support provided by the MRTN-CT-035459 GLADNET project, useful discussions with E. Steers, A. Bogaerts, and K. Rózsa, as well as the contributions of P. Horváth, J. Thoman Forgács, J. Tóth, Gy. Császár, and E. Sárközi to the construction of the experimental apparatus.

[1] K. Danzmann and M. Kock, J. Phys. B **14**, 2989 (1981).
[2] S. Johansson and U. Litzén, J. Phys. B **11**, L703 (1978).
[3] E. B. M. Steers and R. J. Fielding, J. Anal. At. Spectrom. **2**, 239 (1987).
[4] Y. Zhao and G. Horlick, Spectrochim. Acta, Part B **61**, 660 (2006).
[5] E. B. M. Steers, J. Anal. At. Spectrom. **12**, 1033 (1997).
[6] Z. Weiss, J. Anal. At. Spectrom. **21**, 691 (2006).
[7] V. Hoffmann, M. Kasik, P. K. Robinson, and C. Venzago, Anal. Bioanal. Chem. **381**, 173 (2005).
[8] N. H. Bings, A. Bogaerts, and J. A. C. Broekaert, Anal. Chem. **80**, 4317 (2008).
[9] A. Bogaerts and R. Gijebels, Spectrochim. Acta, Part B **53**, 1 (1998).
[10] A. Bogaerts, R. Gijebels, and J. Vlček, J. Appl. Phys. **84**, 121 (1998).
[11] G. Bánó, P. Horváth, T. M. Adamowicz, and K. Rózsa, Appl. Phys. B **89**, 333 (2007).
[12] G. Bánó, L. Szalai, K. Kutasi, P. Hartmann, Z. Donkó, K. Rózsa, A. Kiss, and T. Adamowicz, Appl. Phys. B **70**, 521 (2000).
[13] Z. Donkó, P. Apai, L. Szalai, K. Rózsa, and R. C. Tobin, IEEE Trans. Plasma Sci. **24**, 33 (1996).
[14] F. de Hoog, F. McNeil, F. Collins, and K. Persson, J. Appl. Phys. **48**, 3701 (1977).
[15] G. J. Collins, J. Appl. Phys. **44**, 4633 (1973).
[16] D. C. Gerstenberger, R. Solanki, and G. J. Collins, IEEE J. Quantum Electron. **16**, 820 (1980).
[17] R. Johnsen, J. Macdonald, and M. A. Biondi, J. Chem. Phys. **68**, 2991 (1978).
[18] R. Johnsen, A. Chen, and M. A. Biondi, J. Chem. Phys **72**, 3085 (1980).
[19] J. D. C. Jones, D. G. Lister, and N. D. Twiddy, J. Phys. B **12**, 2723 (1979).
[20] D. L. Smith and J. H. Futrell, J. Chem. Phys. **59**, 463 (1972).
[21] A. R. Turner-Smith, J. M. Green, and C. E. Webb, J. Phys. B **6**, 114 (1973).
[22] R. Johnsen and M. A. Biondi, J. Chem. Phys. **73**, 5045 (1980).
[23] A. Belyaev, J. Phys. B **26**, 3877 (1993).
[24] P. Baltayan, J. C. Pebay-Peyroula, and N. Sadeghi, J. Phys. B **18**, 3615 (1985).
[25] P. Baltayan, J. C. Pebay-Peyroula, and N. Sadeghi, J. Phys. B **19**, 2695 (1986).
[26] K. A. Temelkov, N. K. Vuchkov, R. P. Ekov, and N. V. Sabotinov, J. Phys. D: Appl. Phys. **41**, 105203 (2008).
[27] K. A. Temelkov, N. K. Vuchkov, and N. V. Sabotinov, Plasma Processes Polym. **3**, 147 (2006).
[28] J. A. Rutherford and D. A. Vroom, J. Chem. Phys. **74**, 434 (1981).
[29] E. Steers and A. Thorne, J. Anal. At. Spectrom. **8**, 309 (1993).
[30] K. Wagatsuma and K. Hirokawa, Spectrochim. Acta, Part B **51**, 349 (1996).
[31] R. S. Hudson, L. L. Skrumeda, and W. Whaling, J. Quant. Spectrosc. Radiat. Transf. **38**, 4 (1987).
[32] E. Steers, P. Šmíd, and Z. Weiss, Spectrochim. Acta, Part B **61**, 414 (2006).
[33] V. Weinstein, E. B. M. Steers, P. Šmíd, J. C. Pickering, and S. Mushtaq, J. Anal. At. Spectrom. **25**, 1283 (2010).
[34] A. Bogaerts, K. A. Temelkov, N. K. Vuchkov, and R. Gijbels, Spectrochim. Acta, Part B, **62**, 325 (2007).
[35] G. Bánó, P. Hartmann, K. Kutasi, P. Horváth, R. Plašil, J. G. P. Hlavenka, and Z. Donkó, Plasma Sources Sci. Technol. **16**, 492 (2007).
[36] P. Španěl, Int. J. Mass Spectrom. Ion Process. **149–150**, 299 (1995).
[37] J. Swift and M. J. R. Schwar, *Electrical Probes for Plasma Diagnostics* (Iliffe, London, 1970).
[38] I. Korolov, R. Plašil, T. Kotrík, P. Dohnal, O. Novotný, and J. Glosík, Contrib. Plasma Phys. **48**, 461 (2008).
[39] R. Plašil, I. Korolov, T. Kotrík, P. Dohnal, G. Bánó, Z. Donkó, and J. Glosík, Eur. Phys. J. D **54**, 391 (2009).
[40] L. H. J. Lajunen, *Spectrochemical Analysis by Atomic Absorption and Emission* (Royal Society of Chemistry, Cambridge, 1992).
[41] C. Bruce and P. Hannaford, Spectrochim. Acta, Part B **26**, 207 (1971).
[42] P. Hannaford and D. C. McDonald, J. Phys. B **11**, 1177 (1978).
[43] T. R. O'Brian, M. E. Wickliffe, J. E. Lawler, W. Whaling, and J. W. Brault, J. Opt. Soc. Am. B **8**, 1185 (1991).
[44] D. Engelke, A. Bard, and M. Kock, Z. Phys. D: At., Mol. Clusters **27**, 325 (1993).
[45] S. Krins, S. Oppel, N. Huet, J. von Zanthier, and T. Bastin, Phys. Rev. A **80**, 062508 (2009).
[46] A. Elbern, J. Vac. Sci. Technol. **16**, 1564 (1979).
[47] W. Lindinger and D. L. Albritton, J. Chem. Phys. **62**, 3517 (1975).
[48] Y. Ikezoe, S. Matsuoka, M. Takebe, and A. Viggiano, *Gas Phase Ion-Molecule Reaction Rate Constants* (The Mass Spectroscopy Society of Japan, Tokyo, 1987).
[49] R. Deloche, P. Monchicourt, M. Cheret, and F. Lambert, Phys. Rev. A **13**, 1140 (1976).
[50] X. Urbain, *Dissociative recombination, Theory, Experiment and Applications IV*, edited by M. Larson, J. Mitchell, and I. Schneider (World Scientific, Singapure, 2000).
[51] E. E. Ferguson, F. C. Fehsenfeld, and A. L. Schmeltekopf, Phys. Rev. **138**, A381 (1965).
[52] J. Glosík, G. Bánó, R. Plašil, A. Luca, and P. Zakouřil, Int. J. Mass Spectrom. **189**, 103 (1999).
[53] D. K. Bohme, D. B. Dunkin, F. C. Fehsenfeld, and E. E. Ferguson, J. Chem. Phys. **51**, 863 (1969).
[54] T. Okada and M. Sugawara, J. Phys. D: Appl. Phys. **26**, 1680 (1993).
[55] N. B. Kolokolov and A. B. Blagoev, Phys. Usp. **36**, 252 (1993).
[56] R. Johnsen, A. Chen, and M. A. Biondi, J. Chem. Phys. **73**, 1717 (1980).
[57] I. Korolov, "Recombination and reactions of ions at thermal energies," Ph.D. dissertation (Charles University in Prague, 2008).